Electromagnetic Study of Direct-Driven Wind Turbine Generators by Coupled Field-Circuit Simulations and Full-Scale Bench Tests

Christoph Mülder, Fabian Müller, Andreas Thul and Kay Hameyer
Institute of Electrical Maschines (IEM)
RWTH Aachen University
Aachen, Germany
christoph.muelder@iem.rwth-aachen.de

Christoph Meier
Wobben Research and Development (WRD)
Enercon GmbH
Aurich, Germany
christoph.meier@enercon.de

2021 IEEE Energy Conversion Congress and Exposition (ECCE) | 978-1-7281-5135-9/21/$31.00 ©2021 IEEE | DOI: 10.1109/ECCE47101.2021.9595236

***Abstract*—Studying the electromagnetic behavior of gearless wind turbines, related to parasitic excitation of vibrations and audible noise emission, comes to the fore of science. Reliable simulation and testing methods are essential in this context. The electrical drive train, consisting of the generator that is coupled to a full-scale converter in modern direct-driven turbines, is the first component in the electrical energy supply chain. Particularly, the modeling of its interaction is focused on to study the harmonic content of the generator currents and excited forces in the air gap. Therefore, a weak numerical field-coupling method is used in this contribution to consider both, the current waveform resulting from the coupling and the magnetic forces computed by Finite Element Analyses (FEA). Measurement data, that is collected by means of a 4 MW full-scale test rig, is considered to motivate and validate the proposed model approach. Moreover, the anomalous electromagnetic design of the considered generator is studied by the field-circuit simulation and corresponding magnetic air gap force harmonics are analyzed.**

***Index Terms*—Wind Turbine Generators, Magnetic Forces, Finite Element Analysis, Circuit Coupling.**

I. Introduction

THE problem of modeling electric drive systems in an accurate way has already been addressed by scientific references [1], [2]. Its intention and methodology varies depending on the study in the context of different machine and converter topologies as well as its fields of application.
Speed-variable drives are state-of-the art in many applications [3]. Due to a better aerodynamic efficiency, particularly at partial load and improved controllability, this is the case for modern wind turbines (WTs) [4]. The scope of this work is the interaction of a gearless synchronous generator (SG), its filter and passive rectifier to study its impact on current and force harmonics, exciting additional vibrations and sound emissions of the WT. Beside geometrical effects [5], the occurring current harmonics have to be considered in this context.
As explained in the following methodology chapter, a field-circuit coupling approach is chosen. Starting with a short overview of the theory and field coupling methods from literature, the specific implementation used in the course of this work is expounded.
An experimental study, performed by means of a 4 MW full-scale test bench and a direct driven electrically excited synchronous generator (ESG) as the Device Under Test (DUT), is presented in the third chapter. Electric and mechanic measurement data of the characteristic line, with particular focus on the current waveform, is presented and further analyzed by the example of two operating points.
On this basis, the results and discussion chapter with the model validation follows. Firstly, the sensitivity of the electromagnetic quantities towards simulation parameters, namely the time increment of the FE-simulation, of the chosen field-circuit approach is studied. Secondly, geometrical anomalies of the SG, causing asymmetrical current distributions in the stator winding systems and additional air gap force modes, are analyzed by the proposed model. Finally, the results and findings are concluded in the last section.

II. Methodology

A. Field Coupling Methods

The precise computation of magnetic fields and forces in electrical machines in their respective operating range has to consider not only the machine itself, but the electric environment as well. To enable a communication between the electric circuit and the electric machine, an interface is defined between the different simulation domains [3].
Several methods coupling the electric and magnetic domain in different stages of the computation process exist [6], e.g. strong or weak coupling in the processing stage or post-processing approaches. While post-processing estimations are applicable for active converters [7], they are not applicable for the passive rectifiers, because the switching time instances depend on the magnetic field. The strong coupling of both domains introduces the electrical equations in the Finite-Element-Method (FEM). It is unavoidable to solve the complete system of equations for each time instance, which shall be modeled in the electric circuit, leading to large degrees of freedom; This results in high computational effort. An

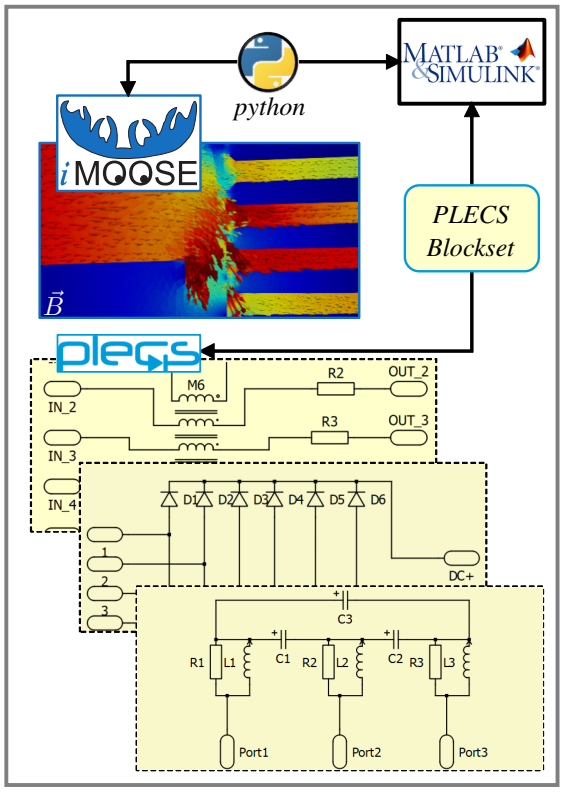

Fig. 1. Implementation of coupled field-circuit simulation in different software packages with interface in MATLAB®&SIMULINK®.

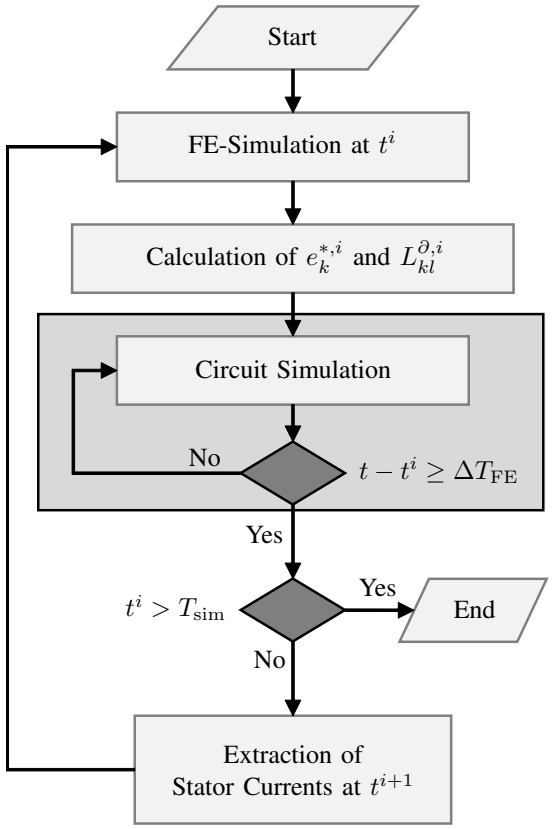

Fig. 2. Flow chart of coupled field-circuit simulation.

efficient way to cope with this problem is the weak coupling, which solves the electrical circuit equations and magnetic field problem separately, but considers the magnetic field state by a linearization of the inductances. This enables the use of different time step widths for each domain. However, a reasonable ratio between the electric and magnetic time step width needs to be employed to avoid inaccuracies due to the linearization. [8].

B. Implementation

The coupling between the magnetic and electrical domain is realized by Simulink$^{\mathrm{TM}}$, which is illustrated in Fig. 1. It triggers the Finite-Element-Analysis (FEA) of the 2D-machine model and the circuit simulation. The FEA is conducted in the IEM-inhouse software iMOOSE / pyMOOSE, while the electric equations are solved by PLECS$^{\mathrm{TM}}$ [9]. By considering the time constants, it can be stated that the electric domain switches its state much faster than the magnetic domain. This results in several electric computations before a new magnetic simulation is triggered, which reduces the computational effort significantly compared to a strong coupling. In the context of the weak coupling, the current is chosen as the state variable for the Finite Element(FE)-model representation.
The phase voltages of the stator are given by

$$u_k = \partial_t \psi_{kl} + R_k i_k \ . \tag{1}$$

ψ_{kl} represents the flux linkage in phase k generated by a current i_l of phase l and the magnetic rotor field at an angular rotor position α and R_k is the ohmic resistance. Applying the temporal derivative on ψ leads to

$$\partial_t \psi_{kl} = L_{kl}^{\partial}(\partial_t i_k) + \omega_{\mathrm{mech}} e_k^* . \tag{2}$$

L_{kl}^{∂} is the tangent inductance matrix and $\omega_{\mathrm{mech}} e_k^*$ is the motion induced electromotive force [3]. Finally, it is possible to determine the current of phase k with (3).

$$i_k = \left(L_{kl}^{\partial}\right)^{-1} \int \left(u_k - R_k i_k - \omega e_k^*\right) \mathrm{d}t. \tag{3}$$

In Fig. 2, the flow chart of the field-circuit coupled simulation and its implementation in different simulation environments is illustrated.
The choice of ΔT_{FE} is particularly of interest [10], since it determines the degree of the linearization of the generator model in the equivalent circuit that shall be sufficient to characterize the occurring current and force harmonics respectively. The time increment ΔT_{circ} of the circuit simulation can be chosen variably as an integer factor considering the harmonic behavior of the studied circuit consisting of filter components and the diode bridge rectifier.

C. Magnetic Field Simulation

The FEA conducted in this contribution is based on the magnetostatic vector potential ($\boldsymbol{A}$-) formulation which originates

from Ampères law:

$$\nabla \times (\nu \nabla \times \boldsymbol{A}) = \boldsymbol{J}, \tag{4}$$

where ν is the magnetic reluctivity of the considered materials and $\boldsymbol{J}$ is the electrical source current densities, that can be derived by the currents in the rotor and stator winding systems respectively. The latter is extracted from the circuit simulation. To model the rotational movement, a sliding interface technique is employed, to enable arbitrary rotor positions without mesh limitations [11], which would state restrictions on the time step size of the simulation domains. The FEA is started each time the trigger is met, to extract the machine quantities such as the inductances and induced voltages.

III. Experimental Study

A. Setup

For the experimental study, measurement data from a test campaign at a 4 MW full-scale test bench [12] is analyzed. In Table I data of the studied wind turbine generator are listed. The device under test (DUT) is a commercial gearless wind turbine equipped with an electrically excited synchronous generator and has a rated apparent power at the grid terminal point S_N of 3.8 MVA. A picture of the test bench setup is shown in Fig. 3. The direct-drive motor (DD-Motor), which is located on the left outside of the picture, is connected by the illustrated yellow shaft of 900 mm of diameter with the DUT. Between the drive and the DUT is an oil-hydraulic non-torque load unit, enabling to load the shaft of the DUT in all six degrees of freedom. These mechanical loads are not studied in this work.

TABLE I
Wind Turbine- and Generator Data.

Quantity	Symbol	Value	Unit
Rated Apparent Power	S_N	3.8	MVA
Rated Speed	n_N	13.1	rpm
Number of Poles	$2p$	96	-
Number of Phases	m	$4 \cdot 3$	-

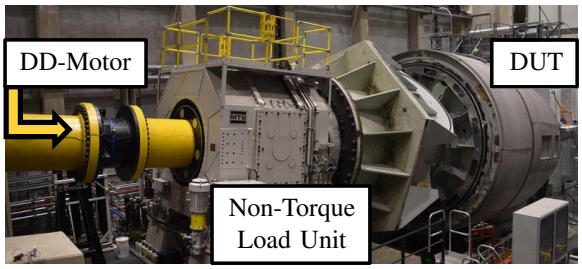

Fig. 3. Test bench setup.

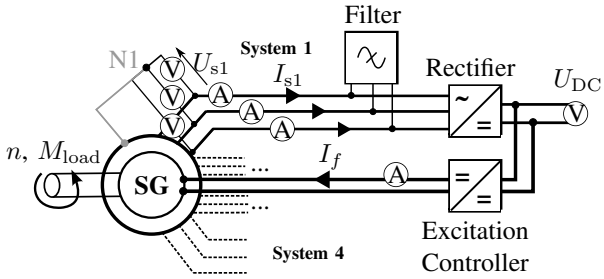

Fig. 4. Schematic circuit diagram of the generator system: Rotor- and stator (System 1) measuring points.

B. Measurement

For the validation of the presented model, generator and test bench quantities, that are both mechanical and electric, are measured. These are

- the rotational speed n, that is identical for both the DD-test bench motor and the DUT,
- the mechanical load torque of the DD-motor M_load,
- the stator line voltages U_{sk},
- the stator phase currents I_{sk},
- the rotor excitation current I_f and
- the rectifier output voltage U_DC.

The mechanic and electric measuring quantities are sampled with a frequency of 0.3 kHz and 4.8 kHz respectively.
In Fig. 4, a schematic circuit diagram of the generator system with the studied measuring points exemplary for phase 1 of stator system 1 is illustrated. The star connection point N1 is indicated for this system and the four three-phase systems are each Y-connected.

C. Testing and Results

For the study of the electromagnetic generator behavior, the nominal characteristic curves of the WT are measured. This is done by reference setting of laminar wind speeds (without any turbulences) at equidistant intervals emulated by the HiL-system of the test bench. Therefore, steady-state operating conditions can be achieved. Additionally, the DUT is parameterized to operate at rated conditions without e.g. reducing its output power.
In Fig. 5, normalized measured quantities of the characteristic curve are illustrated. The analysis, which is performed in the course of this work, refers to two exemplary operating points (OPs) of the rated characteristic curve, that are marked in Fig. 5, to analyze two effects occurring for this topology. Firstly the magnetic circuit of the generator is saturated differently since the excitation current changes. Secondly, the filter has a frequency-dependent transfer behavior, that takes effect due to the different rotational speeds of the synchronous generator along its operational characteristic curve.

In Fig. 6, the normalized stator currents, stator line voltages, stator line-to-line voltages and the rectifier output voltage of one exemplary system over normalized time relative to the electric period time T_el for OP2 are illustrated. The switching

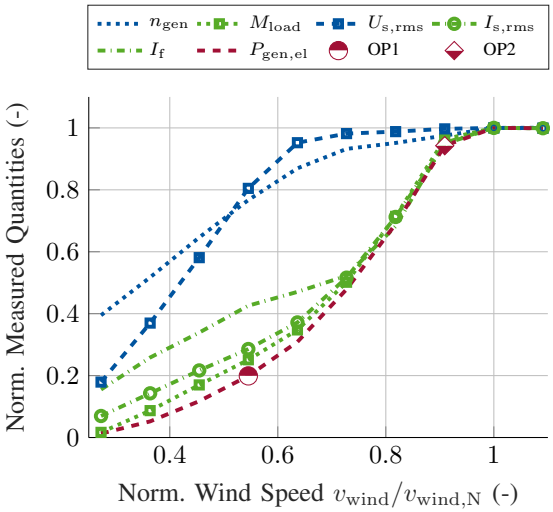

Fig. 5. Normalized measured generator quantities along the operating characteristic curve depending on the emulated laminar wind speed with two marked operating points.

time instances of the rectifier bridge equipped with passive power electronic components are visible. The corresponding commutation processes lead to a distortion of the currents. The smooth course of the rectifier output results from the second system that feeds the DC-link of the rectifier.

The corresponding line-to-line voltages are shifted by 15 °el. equaling $\Delta t/T_{\mathrm{el}} = 0.0416...$. Beside the results for OP2 (Fig. 7b), the currents for OP1 are plotted in Fig. 7a. The current amplitudes are asymmetrical within each system. The impact is under the scope of the next section, where the results of the proposed simulation approach are discussed and compared to measurements.

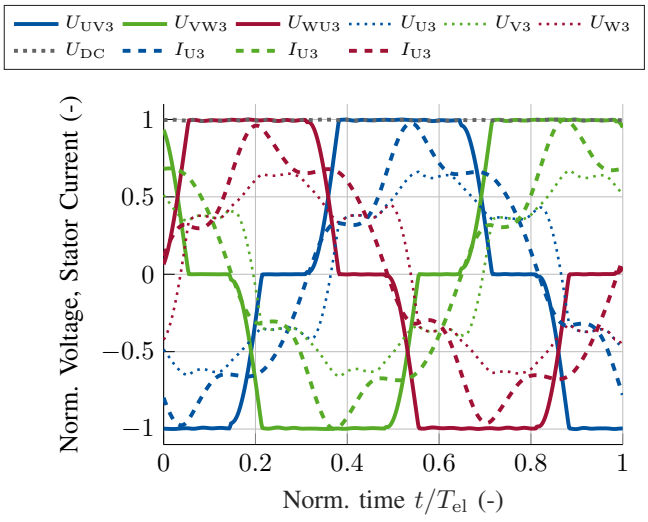

Fig. 6. Normalized stator currents, stator line-, stator line-to-line voltages and rectifier output voltage of System 3 over time for OP2 (see Fig. 5).

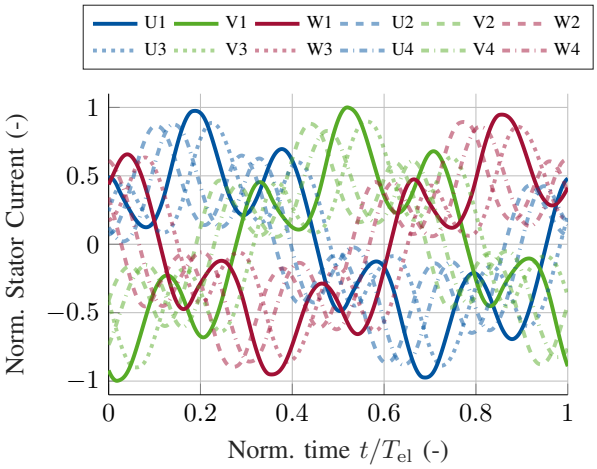

(a) OP1.

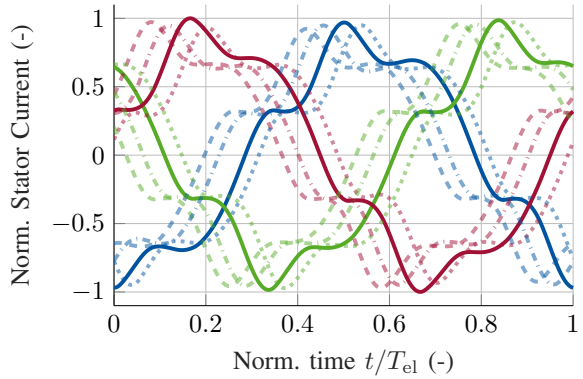

(b) OP2.

Fig. 7. Normalized measured stator currents of all four three-phase systems for the operating points marked in Fig. 5.

IV. Results and Discussion

A. Time Increment of the FE-Simulation

As introduced in section II-A, a weak numerical coupling method is used in the course of this work, since it has the advantage of choosing the time increments of the magnetic (FE-)simulation and the electric (circuit) simulation independently. Since the computational time of the circuit simulation is negligibly small compared to the FEA, different FE-time increments,

$$\Delta T_{\mathrm{FE}} = \frac{T_{\mathrm{el}}}{n_{\mathrm{FE}}}, \tag{5}$$

where n_{FE} is the number of triggered FE-simulations per electric period, are analyzed.

For this initial study, a partial FE-model of one pole pair is simulated, assuming that it corresponds to the smallest symmetrical unit and that the stator is wired with two three-phase systems. In turn, this leads to a significant reduction of the computational effort. The real geometry, having asymmetries due to a lamination with anomalies and having the wiring consisting of 4 systems, as presented in the measurement setup of Fig. 4, is studied in the next section.

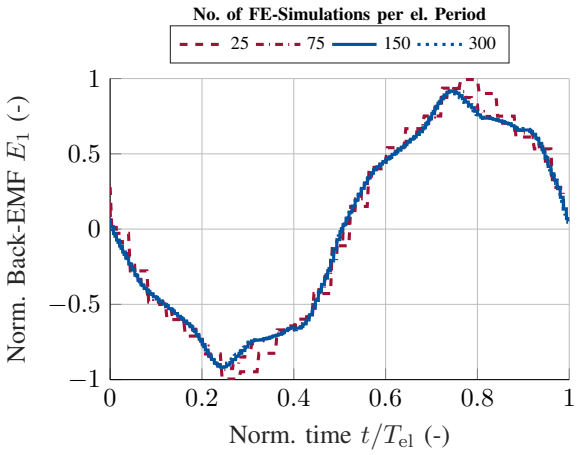

(a) Back-EMF.

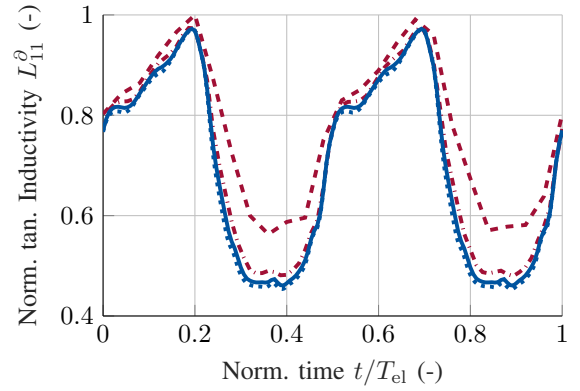

(b) Tangential self-inductance.

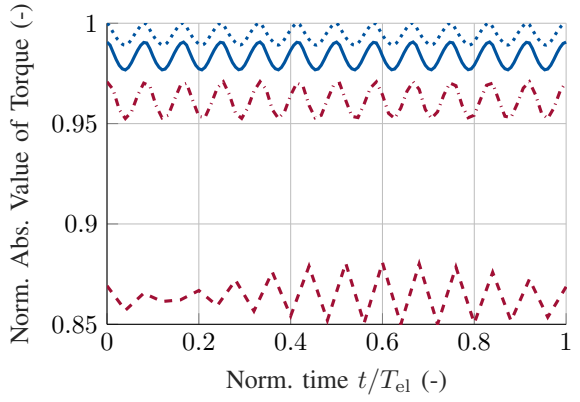

(c) Air gap torque.

Fig. 8. Normalized simulated equivalent circuit (lumped) parameters and air gap torque from field-circuit-simulation of symmetrical FE-model at OP2 (see Fig. 5).

In Fig. 8, the normalized simulated equivalent circuit parameters used in the circuit simulation as stated in (3) and air gap torque are illustrated for four different values of $n_{\mathrm{FE}} = 25, 75, 150$ and 300. The electromotive force (Fig. 8a) that is the input voltage of the circuit simulation, changes significantly between 25 and 75 steps, but has almost the same shape for 150 and 300 steps respectively. The same observation can be made for the course of the tangential self-inductance (Fig. 8b), that is equal for all phases in case of a symmetrical model. The results for the air gap torque show that both the oscillation and the mean value change for different time increments. For 25 steps it shows an asymmetric course, since the slot harmonics are undersampled and the mean value is significantly smaller. The difference between 75 and 150 steps decreases. This trend is continued further for $n_{\mathrm{FE}} = 300$. Moreover, the torque oscillation reduces monotonously. The stated findings can be explained by the simulated currents computed for the respective FE-time increments.

After considering the global torque of the machine, the local sum force, both in radial and tangential direction, acting on a single tooth that are plotted in normalized representation in Fig. 9, is studied at OP2. Both components only differ significantly between the coarsest (with 25 steps) and the other time increments.

The normalized currents of one phase and the line-to-line voltage of two exemplary phases are plotted in Fig. 10.

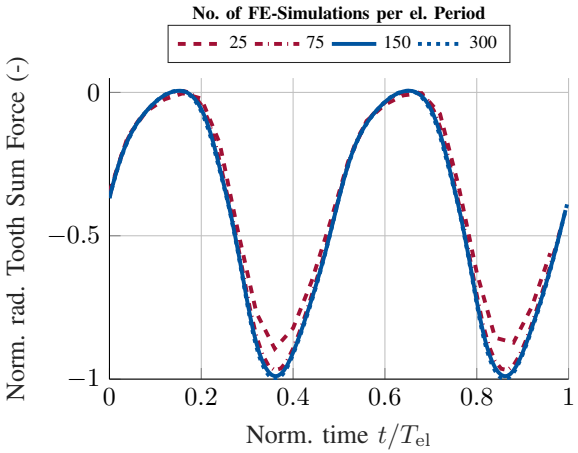

(a) Radial.

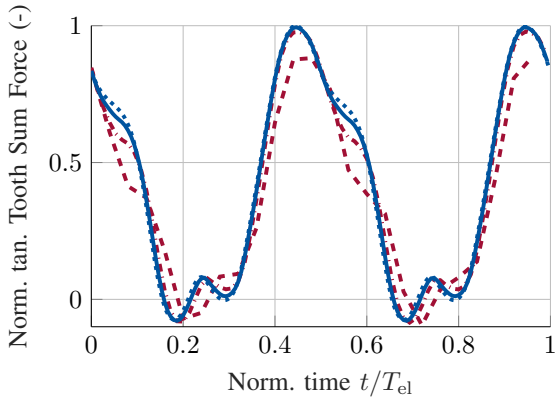

(b) Tangential.

Fig. 9. Normalized tooth sum forces over time from field-circuit-simulation of symmetrical FE-model at OP2.

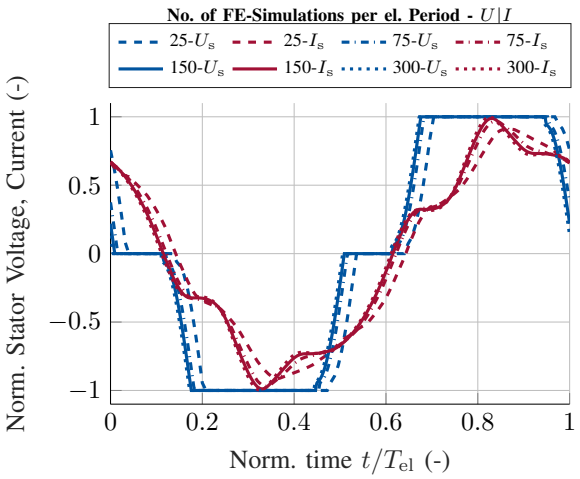

Fig. 10. Normalized stator line-to-line voltage and current of phase 1 over time for OP2 (see Fig. 5).

The amplitude of the currents increase with more steps per period, since the current-slopes are locally larger due to smaller inductivities (see Fig. 8b). This can be correlated to the torque results as stated before. The current waveforms differ accordingly. When analyzing the line-to-line voltage, different commutation time instances can be observed.
In conclusion, a time step number of 150 per electric period turns out to be sufficient since by choosing more or rather doubling the results change only slightly. For the comparison with measurments and further study of the asymmetric model in the next section, this value is therefore chosen.

In Fig. 11b, the simulated and measured normalized stator line-to-line voltages and currents for OP2 are plotted. Both, the measured currents and line-to-line voltages are asymmetrical. The best accordance for the voltages is for U_{WU}. The current amplitudes however deviate, whereas the shape is approximated sufficiently. This result is in turn essential for the harmonic field analysis. The deviation can have several reasons, e.g. geometrical 3D-effects (skewing, winding head), different magnetic material or power electronic behaviors, that cannot be considered by 2D-FEA models or circuit simulators. The study of these effects will not be under the scope of this contribution.
In Fig. 12, the normalized frequency spectra of simulated and measured stator currents at both studied operating points are illustrated. Analogous to the findings of the time course analysis, the dominant frequency order, that are the fundamental and fifth harmonic, excited by the six switching or rather commutation processes per electric period, are in good accordance. The harmonic orders above seven are significantly smaller due to filtering. Secondly, it can be concluded that the impact of the rectifier and filter on the occuring stator current harmonics depends significantly on the operating point. Therefore, the analysis of the electromagnetic generator behavior has to consider this coupling.

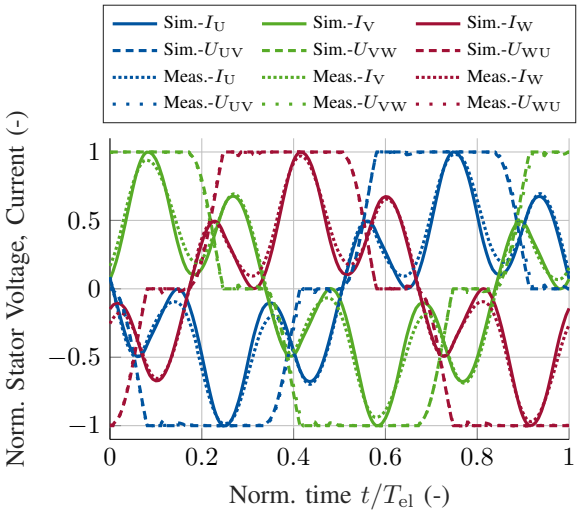

(a) OP1.

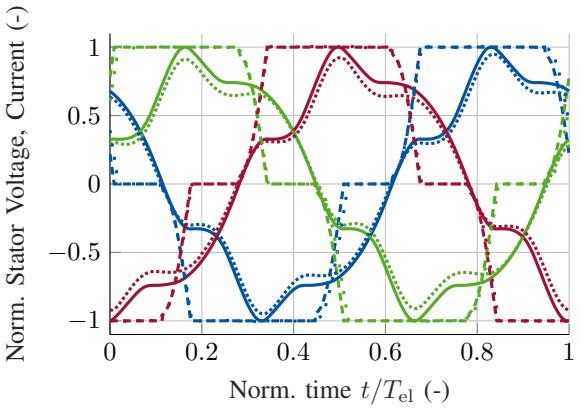

(b) OP2.

Fig. 11. Simulated (Sim.) and measured (meas.) normalized stator line-to-line voltages and currents over time.

B. Anomalous Electromagnetic Generator Design

1) Geometry and Field Solution

As explained in section III-B, the stator winding consists of four three-phase systems. The corresponding strands are wound over the full circumference of the machine. These alternations take place at anomalous parts of the stator lamination, namely a double-tooth and a double-slot, that are illustrated in Fig. 13. Each two systems alternately are inserted in the slots of the intermediate area (between two anomalies). Consequently, the smallest symmetry of the geometry is not one pole pair as assumed in the previous section, but one eigth of the circumference. The corresponding 2D-FE-model with the normalized magnetic flux density solution and flux lines at an exemplary time step of OP2 is plotted in Fig. 14. The asymmetric shape of the magnetic field is recognizable, when comparing adjacent magnetic poles in the stator along the circumference.
In the next section, both the spatial and time behavior of

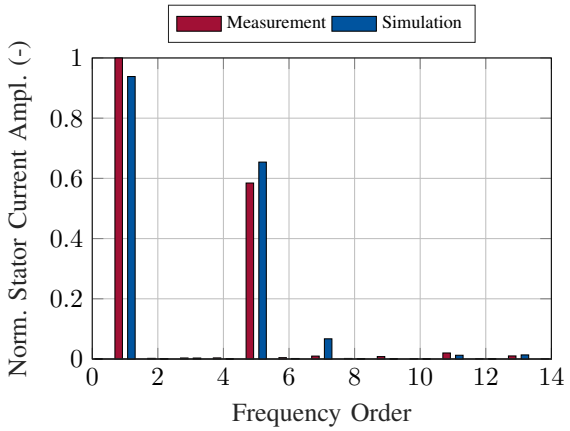

(a) OP1.

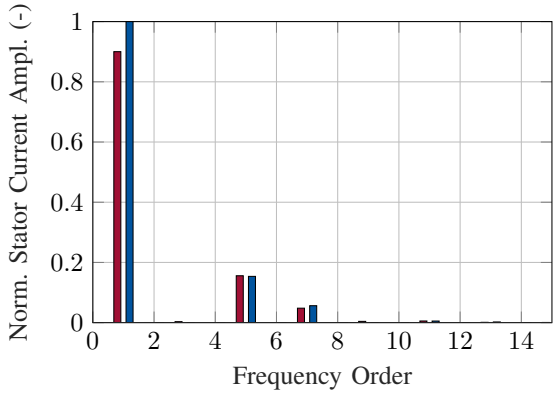

(b) OP2.

Fig. 12. Normalized frequency spectra of simulated and measured stator currents at studied operating points.

the magnetic forces, which are excited in the air gap of the generator, are therefore studied.

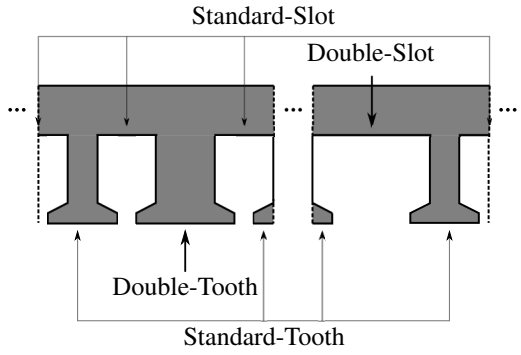

Fig. 13. Schematic sketch of lamination cross sections with anomalies of asymmetric electromagnetic generator design.

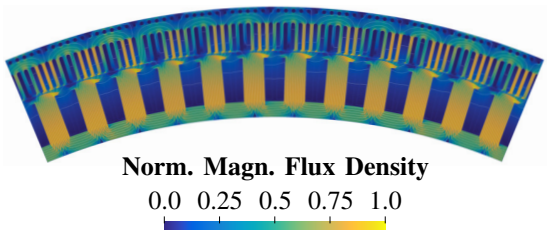

Fig. 14. Normalized magnetic flux density solution and flux lines of 2D-FE generator model with anomalies at OP2.

2) Analysis of Air Gap Force Harmonics

To study the impact of non-sinusoidal current waveform on corresponding force harmonics of the generator, one-sided 2D-force density spectra derived from the spatial- and time-distributed magnetic air gap field of the generator and computed by the Maxwell stress tensor are analyzed. To evaluate the tangential force density orders occurring due to the anomalies, as described in the previous section, and those due to circuit-coupling, the generator is analyzed initially for ideal sinusoidal current supply.

The result for OP2 is plotted in Fig. 15. Secondly, the same quantity is computed by the circuit-coupled simulation with the derived parameters. The force density spectrum is plotted in Fig. 16. The spatial orders $-10 \leq \eta \leq 10$ are considered, since they are dominant in terms of the vibration behavior [13].

Both spectra show the spatial order of eight, resulting from the anomalies. Moreover, frequency orders corresponding to the breathing mode ($\eta = 0$) occur, that are particularly crucial in the application context [14]. When comparing the results for both current supply methods, particularly the spectrum obtained by circuit-coupled simulations show larger amplitudes of higher frequency orders ($\nu/p > 10$). Moreover, the

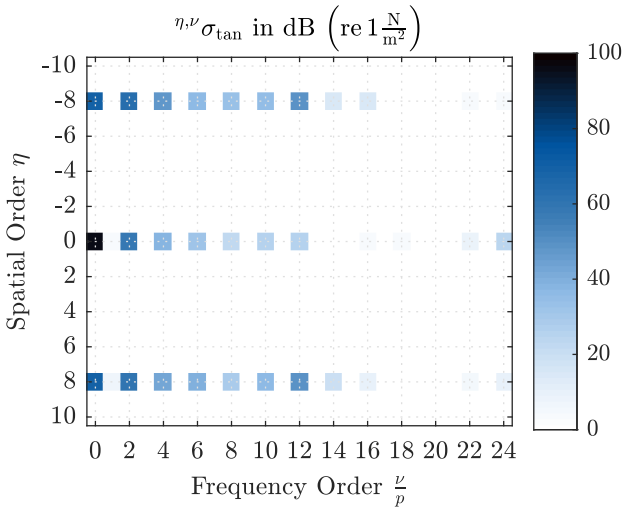

Fig. 15. Tangential air gap force density spectrum simulated for ideal sinusoidal stator current feeding at OP2.

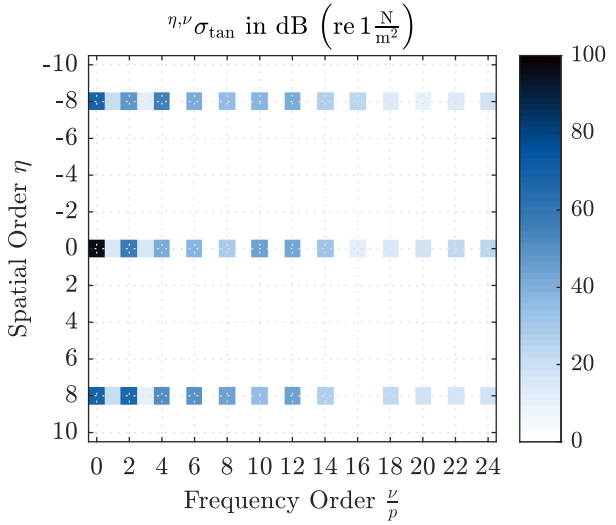

Fig. 16. Tangential air gap force density spectrum simulated for circuit-coupled stator current feeding at OP2.

spatial order $\eta = 8$ shows different values for the considered frequencies. Active inverter topologies and control strategies aim at suppressing parasitic modes and frequencies [15].

V. Conclusions

This work studies the electromagnetic behavior of a direct-driven wind turbine generator by a field-circuit coupling approach and full-scale test bench measurements. It focuses on parasitic force excitation originating from the interaction of the generator with its connected circuit, namely the filter and rectifier. Therefore, an efficient, weak-coupled method, enabling the choice of different time step widths in the electric and magnetic domain respectively, is introduced. Based on the utilized machine equations, the lumped parameters, namely the back-EMF and tangential inductances which are computed by the magnetic FEA, are explained. Afterwards, the fundamentals of the FEA, whereby magnetic forces are computed in the postprocessing, are stated. The measurement quantities of the experimental study, which is performed on a 4 MW full-scale test bench, are evaluated along the characteristic line of the DUT. Time courses of two exemplary operating points are studied. These are subsequently compared to the results obtained by the simulation approach, after performing a sensitivity analysis of several electromagnetic quantities towards the FE-time step width. Finally, the anomalous electromagnetic generator design is explained and its magnetic forces densities are studied by 2D (space/time)-spectra for sinusoidal and circuit-coupled current supply.

Acknowledgment

This research was funded by Federal Ministry for Economic Affairs and Energy of Germany. We also thank our project partners, who provided equipment, insight and expertise that greatly assisted the research.

Supported by:

Federal Ministry for Economic Affairs and Energy

on the basis of a decision by the German Bundestag

References

[1] M. van der Giet, E. Lange, D. A.P. Correa, I. E. Chabu, S. I. Nabeta, and K. Hameyer, "Acoustic simulation of a special switched reluctance drive by means of field-circuit coupling and multiphysics simulation," IEEE Transactions on Industrial Electronics, vol. 57, no. 9, pp. 2946-2953, 2010.

[2] J. Wu, J. Wang, C. Gan, Q. Sun, and W. Kong, "Efficiency optimization of PMSM drives using field-circuit coupled FEM for EV/HEV applications," IEEE Access, vol. 6, pp. 15192– 15201, 2018.

[3] T. Herold, E. Lange, and K. Hameyer, "System simulation of a PMSM servo drive using field-circuit coupling," IEEE transactions on magnetics, vol. 47, no. 5, pp. 938–941, 2011.

[4] J. A. Baroudi, V. Dinavahi, and A. M. Knight, "A review of power converter topologies for wind generators," Renewable energy, vol. 32, no. 14, pp. 2369–2385, 2007.

[5] C. Mülder, T. Duda, G. Jacobs, and K. Hameyer, "Model approach for electromagnetically excited mechanical vibrations in direct-drive wind turbines," J. Phys.: Conf. Ser., vol. 1618, no. 2, p. 22060, 2020.

[6] K. Hameyer, J. Driesen, H. de Gersem, and R. Belmans, "The classification of coupled field problems," IEEE transactions on magnetics, vol. 35, no. 3, pp. 1618–1621, 1999.

[7] M. Jaeger, S. Rick and K. Hameyer, "Current Simulation of a Controlled PMSM Including Skew and Torsional Rotor Vibrations," in 2018 XIII International Conference on Electrical Machines (ICEM), pp.111-117, 2018.

[8] E. Lange, F. Henrotte, and K. Hameyer, "An efficient field-circuit coupling based on a temporary linearization of FE electrical machine models," IEEE transactions on magnetics, vol. 45, no. 3, pp. 1258–1261, 2009.

[9] J. H. Alimeling and W. P. Hammer, "PLECS-piece-wise linear electrical circuit simulation for Simulink," in Proceedings of the IEEE 1999 International Conference on Power Electronics and Drive Systems. PEDS'99 (Cat. No. 99TH8475), 1999, pp. 355–360.

[10] S. Kanerva, S. Seman, and A. Arkkio, "Simulation of electric drive systems with coupled finite element analysis and system simulator," in 10th European Conference on Power Electronics and Applications (EPE 2003), 2003, pp. 2–4.

[11] E. Lange, F. Henrotte and K. Hameyer, "A Variational Formulation for Nonconforming Sliding Interfaces in Finite Element Analysis of Electric Machines," in IEEE Transactions on Magnetics, vol. 46, no. 8, pp. 2755-2758, Aug. 2010.

[12] N. R. Averous et al., "Development of a 4 MW Full-Size Wind-Turbine Test Bench," IEEE Journal of Emerging and Selected Topics in Power Electronics, vol. 5, no. 2, pp. 600–609, 2017.

[13] T. Duda, C. Mülder, G. Jacobs, K. Hameyer, D. Bosse, and M. Cardaun, "Integration of electromagnetic finite element models in a multibody simulation to evaluate vibrations in direct-drive generators," (in En;en), Forsch Ingenieurwes, vol. 85, no. 2, pp. 257–264, 2021.

[14] J. Andresen, S. Vip, A. Mertens, and S. Paulus, "Compensation of the Radial and Circumferential Mode 0 Vibration of a Permanent Magnet Electric Machine based on an Experimental Characterisation," in 2020 22nd European Conference on Power Electronics and Applications (EPE'20 ECCE Europe), 2020, P.1-P.9.

[15] J. Andresen, S. Vip, A. Mertens, and S. Paulus, "Theory of Influencing the Breathing Mode and Torque Pulsations of Permanent Magnet Electric Machines with Harmonic Currents," in 2020 22nd European Conference on Power Electronics and Applications (EPE'20 ECCE Europe), 2020, P.1-P.9.